PCCP

Accepted Manuscript

ROYAL SOCIETY OF CHEMISTRY

www.rsc.org/pccp

Physical Chemistry Chemical Physics

Cite this: DOI: 10.1039/c0xx00000x

ARTICLE

www.rsc.org/xxxxxx

Adsorption of CO_2 on amine-functionalised MCM-41: experimental and theoretical studies

Thiago Custódio dos Santos,[a] Sandrine Bourrelly,[b] Philip L. Llewellyn,[b] José Walkimar de M. Carneiro,[a] and Célia Machado Ronconi*,[a]

Received (in XXX, XXX) Xth XXXXXXXXX 20XX, Accepted Xth XXXXXXXXX 20XX
DOI: 10.1039/b000000x

Adsorption of CO_2 on MCM-41 functionalised with [3-(2 aminoethylamino)propyl] trimethoxysilano (**MCM-41-N2**), N^1-(3-trimethoxysilylpropyl)diethylenetriamine (**MCM-41-N3**), 4-aminopyridine (**MCM-41-aminopyridine**), 4-(methylamino)pyridine (**MCM-41-methylaminopyridine**) and 1,5,7-triazabicyclo[4.4.0]dec-5-ene (**MCM-41-guanidine**) was investigated. The amine-functionalised materials were characterised by ^{29}Si and ^{13}C solid-state nuclear magnetic resonance, N_2 adsorption/desorption isotherms, X-ray diffraction and transmission electron microscopy. CO_2 adsorption at 1.0 bar and 30 ^oC showed that the amount of CO_2 (n_{ads}/mmol g^{-1}) adsorbed on **MCM-41-N2** and **MCM-41-N3** is approximately twice the amount adsorbed on MCM-41. For **MCM-41-aminopyridine**, **MCM-41-methylaminopyridine** and **MCM-41-guanidine**, the CO_2 adsorption capacity was smaller than that of MCM-41 at the same conditions. The proton affinity (computed with wB97x-D/6-311++G(d,p)) of the secondary amino groups is higher than that of the primary amino groups; however, the relative stabilities of the primary and secondary carbamates are similar. The differential heat of adsorption decreases as the number of secondary amino groups increases.

Introduction

To satisfy the increasing demand for energy due to population and economic growth, industrial processes and fossil fuel combustion have released an unprecedented amount of CO_2 into the atmosphere. The following sectors are mainly responsible for CO_2 emissions: energy supply (47%), industry (30%), transportation (11%) and buildings (3%). In the past decade, CO_2 emissions increased by 1.0 gigatonne carbon dioxide equivalents ($GtCO_2eq$) per year compared to 0.4 $GtCO_2eq$/year from 1970 to 2000. In 2010, 49 (± 4.5) $GtCO_2eq$ was released into the atmosphere, which is considered the highest emission value reported in human history. Considering this scenario, several mitigation policies have been proposed in the Intergovernmental Panel on Climate Change (IPCC) 2014 report to stabilise CO_2 concentrations in the range of 430-530 ppm by the end of this century. To reach this level, special attention needs to be given to the carbon energy supply sector, particularly coal-fired power plants. Therefore, the search for efficient methods for the large-scale capture and separation of CO_2 from fossil fuel power plants, refineries, oil and gas extraction sites is a challenge that needs to be addressed to reduce CO_2 emissions into the atmosphere.[1,2]

The current technology based on aqueous alkanolamine solutions, such as 2-aminoethanol (MEA), 2,2-iminodiethanol (DEA), 2,2-methyliminodiethanol (MDEA), 1-(2-hydroxypropylamino)propan-2-ol (DIPA), and 2-amino-2-methylpropan-1-ol (AMP), for CO_2 removal was established in 1930.[3,4] However, issues related to the high costs and environmental impacts of these alkanolamine solutions due to the corrosive nature of the amines, high regeneration energy in the CO_2 stripping step and formation of nitrosamines (carcinogens) due to amine thermal decomposition are among the biggest challenges of this technology. An alternative to aqueous alkanolamine solutions can be to graft amines (primary, secondary or tertiary) onto solid supports, such as mesoporous silica nanoparticles (MCM-41, SBA-15),[5,6,7] zeolites,[8] Metal Organic Frameworks (MOFs),[9] TiO_2,[10] and clays.[11] This approach is particularly interesting for CO_2 uptake at low partial pressures. In addition, it can reduce the energy costs in the CO_2 stripping step and also the carcinogenic products resulting from the amine thermal degradation can be avoided.[12]

MCM-41 is a particularly interesting support to attach amines to either by impregnation or post-synthetic grafting because of its high surface area (~ 1000 m^2 g^{-1}), high pore volume (~ 1.07 cm^3 g^{-1}), regular pore size (~ 3.0 nm) and ease of surface functionalisation[13,14,15]. Several papers have reported that MCM-41 and pore-expanded MCM-41 have been modified with primary, secondary, tertiary and polyamines.[5,16] Sayari *et al.*[16] showed that primary amines anchored onto pore-expanded MCM-41 had higher CO_2 adsorption capacity than secondary amines, whereas the tertiary ones barely reacted. This result is interesting because the basicities of secondary and tertiary amines are higher than that of

the primary ones. Svendsen *et al.*[17,18] showed that the reaction between CO_2 at low loadings and an aqueous solution of 2-((2-aminoethyl) amino)-ethanol ($H_2N(CH_2)_2NH(CH_2)_2OH$, AEEA) – which has one primary and one secondary amine groups in its structure – yielded mainly the primary carbamate of AEEA. The secondary carbamate and the dicarbamate of AEEA were detected in negligible amounts. They concluded that the primary group reacts faster than the secondary group. Monte Carlo simulation of amine-functionalised silica materials indicated that both chemisorption and physisorption processes play a role in the interaction of CO_2 with the surface and that functionalisation makes the CO_2-surface interaction stronger.[19]

Previously, using the CAM-B3LYP/6-311++G(2d,2p) approach, we have investigated the interaction between CO_2 and a set of primary, secondary and tertiary amines to form a zwitterion intermediate. We found an almost linear correlation between the CO_2 interaction energies and the amine basicities.[20] In this work, the synthesis, characterisation, CO_2 uptake and CH_4 uptake by a set of amines anchored onto commercially available MCM-41 are discussed. The relationship between amino efficiency, differential heat of adsorption and basicity (calculated using wB97x-D/6-311++G(d,p) method) for some of those anchored amines are provided.

Experimental

Materials

The following chemicals were used with no further treatment: [3-(2-aminoethylamino)propyl]trimethoxysilano, N^1-(3-trimethoxysilylpropyl)diethylenetriamine, (3-chloropropyl)triethoxysilane, 4-aminopyridine, 4-(methylamino)pyridine, 1,5,7-triazabicyclo[4.4.0]dec-5-ene (guanidine), triethylamine, benzophenone and sodium hydride from Sigma-Aldrich, dichloromethane and diethyl ether from Vetec-Brazil. MCM-41 mesoporous silica from Sigma-Aldrich, toluene and tetrahydrofuran (THF) from Vetec-Brazil were dried prior to their use.

Organoalkoxysilane grafting

MCM-41 was grafted with [3-(2-aminoethylamino)propyl]trimethoxysilano, N^1-(3-trimethoxysilylpropyl)diethylenetriamine) and (3-chloropropyl)triethoxysilane by a post-synthesis method[5,13,14] to give the title compounds **MCM-41-N2**, **MCM-41-N3** and MCM-41-Cl, respectively. Briefly, 6 mL of each organoalkoxysilane was added dropwise to a suspension of MCM-41 (6.00 g) in anhydrous PhMe under reflux (150 mL) in an Ar atmosphere, while stirring vigorously. After 1.5 h, a fraction of 7.0 mL of PhMe containing MeOH or EtOH was distilled off from the suspension, followed by the addition of 3 mL more of each organoalkoxysilane. This procedure was repeated three times, and the reaction mixture was left to stir under reflux and an Ar atmosphere for an additional 24 h. For the MCM-41-Cl compound, this procedure was repeated four times and the suspension heated under reflux for an additional 48 h. The reaction mixtures were cooled to RT, and the resulting suspensions filtered and the excess non-reacted organoalkoxysilane removed by washing the solids in a Soxhlet apparatus using CH_2Cl_2:Et_2O (1:1, 600 mL) for 24 h. The compounds were then dried under vacuum to afford **MCM-41-N2**, **MCM-41-N3** and MCM-41-Cl, as white solids.

Functionalisation of MCM-41-Cl with 4-aminopyridine, 4-(methylamino)pyridine, 1,5,7-triazabicyclo[4.4.0]dec-5-ene (guanidine)

4-aminopyridine (1.0 g, 10.6 mmol) in anhydrous PhMe (5.0 mL) was added to a suspension of MCM-41-Cl (2.0 g) in dry PhMe under reflux (50 mL) and Ar atmosphere while stirring vigorously. After the reaction mixture had been left to stir for 24 h, it was cooled to RT, filtered and the solid subsequently washed in a Soxhlet apparatus using 5% triethylamine in CH_2Cl_2:Et_2O (1:1, 600 mL) for 24 h and then CH_2Cl_2:Et_2O (1:1, 600 mL) for an additional 24 h. This procedure was necessary to activate the material because upon the nucleophilic substitution, the HCl product remains on the solid surface, neutralising the active site. After this treatment, the material was dried under vacuum and named **MCM-41-aminopyridine**.

For the synthesis of **MCM-41-methylaminopyridine**, a solution of 4-(methylamino)pyridine (0.50 g, 4.6 mmol) in 3 mL of anhydrous THF was added dropwise to a suspension of NaH (0.177 g, 7.4 mmol) in 3 mL of anhydrous THF in an ice bath under argon. The suspension was stirred for an additional 2 h at room temperature and then MCM-41-Cl (0.62 g, 0.54 mmol of chlorine) in 4 mL of anhydrous THF was added. The reaction mixture was subsequently heated to 70 °C under an argon atmosphere for 15 h. Upon cooling to RT, the suspension was filtered and the solid subsequently washed in a Soxhlet apparatus using CH_2Cl_2:Et_2O (1:1, 600 mL) for 24 h. The compound was then dried under vacuum at 80 °C for 4 h to afford **MCM-41-methylaminopyridine**.

The synthesis of **MCM-41-guanidine** has been described elsewhere.[13]

Characterisation

Solid-state ^{13}C and ^{29}Si NMR spectra were obtained on a Bruker Avance III spectrometer (9.4T), operating at Larmor frequencies of 100.62 and 79.48 MHz, respectively, and equipped with a 4 mm Bruker CPMAS probe and ZrO_2 rotors, spinning at 10 kHz (^{13}C and ^{29}Si). For ^{13}C NMR spectra, a ^1H-^{13}C cross polarisation magic angle spinning (CPMAS) pulse sequence was employed, with an optimised contact time of 4 ms, and a repetition time (D1) of 1 s. ^{29}Si MAS NMR spectra were acquired by using both ^1H-^{29}Si cross polarisation (CPMAS) with a contact time of 4 ms and direct polarisation, with high power ^1H dipolar decoupling (HPDD) pulse sequences. In the latter case, the experiments were performed by using repetition times of 10 to 300 s. External references: adamantane for ^{13}C and the Q^3 Si sites of kaolinite at –91.5 ppm for ^{29}Si.[5,13,14]

The amounts of carbon, nitrogen and hydrogen were obtained in a Perkin Elmer CHN 240C analyser, and the amount of chlorine in the MCM-41-Cl sample was determined by the volumetric method at the Analytical Centre of the Institute of Chemistry, University of São Paulo, Brazil.

N_2 sorption experiments were carried out in a Micromeritics ASAP 2020 V304 e-serial 1200 apparatus at 77 K. Prior to each sorption experiment, 100 mg of each sample was dried in an oven at 150 °C for 24 h, then introduced into a quartz cell and attached to the physisorption apparatus where they were outgassed under

vacuum for 2 h at 100 °C. X-ray diffraction (XRD) was carried out on a Bruker AXS D8 Advance (Cu Kα radiation, 40 kV and 40 mA). Transmission electron microscopy (TEM) micrographs were acquired using a Carl Zeiss CEM-902 microscope equipped with a Casting-Henry-Ottensmeyer filter spectrometer.

Gas adsorption and calorimetry

The adsorption of methane and carbon dioxide was performed at 30 °C and up to 30 bars. The adsorption isotherms were obtained using a homemade built high-throughput instrument.[21] Gas adsorption is measured on six samples in parallel via a manometric gas dosing system. The amounts of gas adsorbed are calculated by an equation of state using the Reference Fluid Thermodynamic and Transport properties (REFPROP) software package 8.0 of the National Institute of Standards and Technology (NIST).[22] Around 100 mg of sample is used, and each sample is thermally activated individually *in situ* under primary vacuum at a chosen temperature overnight prior gas adsorption measurement. The gases were obtained from Air Liquid: methane was of 99.9995% purity (N55) and carbon dioxide was of 99.995% purity (N45).

The calorimetry experiments were performed using a manometric adsorption apparatus coupled with a Tian–Calvet type microcalorimeter (Setaram, C80). This experimental device allows the determination of the adsorption isotherm and the adsorption enthalpy simultaneously using a point-by-point introduction of gas to the sample. The gas is introduced via a double pneumovalve system into the reference volume. Once the pressure is stabilised in this volume, a pneumovalve is opened to allow the gas to reach the sample. Each introduction of adsorbate to the sample is accompanied by an exothermic thermal effect, until equilibrium is attained. The peak in the curve of energy with time has to be integrated to provide an integral (or pseudo-differential) molar enthalpy of adsorption for each dose. Experiments were carried out at 303 K and up to 30 bars. Approximately 500 mg of the samples were placed in a clean, properly dried high pressure vessel. To compensate for phenomena linked to the vessel and to the injection of gas, a high pressure vacuum vessel was placed in the reference well of the calorimeter.

DFT calculations

To simulate the basicity of the primary *versus* the secondary amino groups, the relative proton affinities of the N^1-ethylethane-1,2-diamine ($CH_3CH_2NH(CH_2)_2NH_2$) and N^1-(2-aminoethyl)-N^2-ethylethane-1,2-diamine ($CH_3CH_2NH(CH_2)_2NH(CH_2)_2NH_2$) were calculated. The relative energy was also computed for the formation of the carbamate in both the primary and secondary positions of the same amines. Geometry optimizations and calculation of absolute energies were performed with the wB97x-D/6-311++G(d,p) combination of functional[23] and basis set, using the G09 suite of programs.[24] To identify the most probable conformation of each protonated amine and carbamates we employed the conformer distribution routine of the Spartan´10 software.[25] The three most stable conformations of each molecule were then fully optimized with the wB97x-D/6-311++G(d,p) method. Calculation of the second order hessian matrix confirmed all the optimized geometries as a true minimum.

Results and discussion

Chemical modification of MCM-41

The synthetic routes to obtain the functionalised materials containing primary, secondary and tertiary amino groups covalently bounded to MCM-41 are outlined in Scheme 1. Commercially available MCM-41 was modified by a post-synthetic method using [3-(2-aminoethylamino)propyl]trimethoxysilano and N^1-(3-trimethoxysilylpropyl)diethylenetriamine) to obtain **MCM-41-N2** and **MCM-41-N3**, respectively (Scheme 1). In this method, the silanol groups that are inside the pores and those on the outer surface are both chemically accessible and may easily react with alkoxysilane derivatives to introduce organic functionality onto the MCM-41. To avoid autocondensation of the alkoxysilanes, the reaction was carried out under anhydrous conditions, and the excess unreacted alkoxysilanes were removed by washing the solids in a Soxhlet apparatus. This procedure was conducted to ensure that only covalently bounded amino groups would be grafted on the MCM-41. The **MCM-41-aminopyridine**, **MCM-41-methylaminopyridine** and **MCM-41-guanidine** materials were obtained by bimolecular nucleophilic substitution reactions (S_N2) between the MCM-41-Cl and the respective amines, Scheme 1.

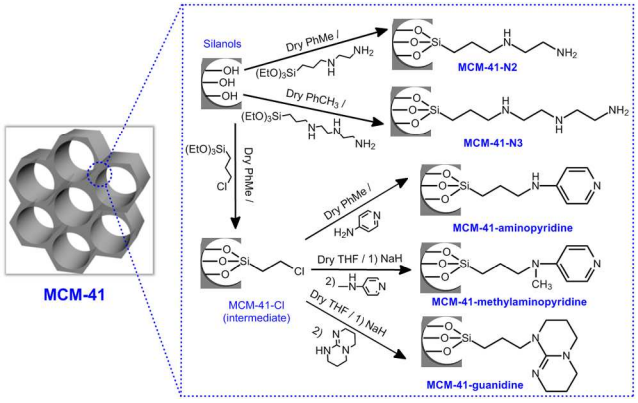

Scheme 1. The functionalisation of MCM-41 with [3-(2-aminoethylamino)propyl]trimethoxysilano (**MCM-41-N2**), N1-(3-trimethoxysilylpropyl)diethylenetriamine) (**MCM-41-N3**), (3-chloropropyl)triethoxysilane (MCM-41-Cl), 4-aminopyridine (**MCM-41-aminopyridine**), 4-(methylamino)pyridine (**MCM-41-methylaminopyridine**) and 1,5,7-triazabicyclo[4.4.0]dec-5-ene (**MCM-41-guanidine**).

Characterisation of the amine-functionalised materials

The ^{29}Si CPMAS NMR spectrum of MCM-41 (Fig. 1) exhibits signals at –92 and –100 ppm that are associated with the silanol groups $SiO_2(OH)_2$ (Q^2 sites) and SiO_3-OH (Q^3 site), respectively.[5,13,14] A signal at –113 ppm, associated with the siloxane group SiO_4 (Q^4 site), was also observed. In addition to the Q^4, Q^3 and Q^2 sites, all the amine-functionalised materials also exhibit T^3, (C-Si(OSi)$_3$), and T^2, (C-Si(OSi)$_2$OH), sites in the range of –63 to –75 ppm and –62 to –54 ppm, respectively. T^n sites indicates the presence of organic groups covalently bound to the MCM-41.

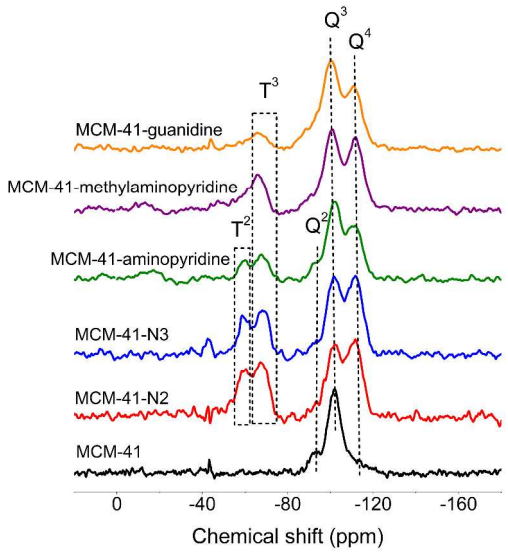

Fig. 1 ^{29}Si CPMAS NMR spectra of MCM-41 and amine-functionalised samples.

The ^{13}C CPMAS NMR spectra of **MCM-41-N2** and **MCM-41-N3** present four (C1 (6.8 ppm), C2 (18.3 ppm), C3, C4 (35.7 ppm), C5 (48.0 ppm)) and five (C1 (6.8 ppm), C2 (17.6 ppm), C3 (36.4 ppm), C4, C5, C6 (43.6 ppm), C7 (48.0 ppm)) signals, respectively (Fig. 2). In these spectra, C1 is the most shielded by being directly bound to the silicon atom whereas C3, C4 (**MCM-41-N2**) and C4, C5 and C6 (**MCM-41-N3**) are assigned to the carbon atoms bound to the amino groups (NH and NH_2), following the literature assignments for MCM-41 functionalised with an organoalkoxysilane by the co-condensation method.[26] One signal approximately 162 ppm was assigned to the formation of carbamate, probably due to the reaction of atmospheric CO_2 with amino groups anchored onto the surface of the materials.[5,16] For the **MCM-41-methylaminopyridine**, signals related to the aliphatic carbons are observed at 5.9 ppm (C1), 21.6 ppm (C2) and 57.3 ppm (C3). For **MCM-41-methylaminopyridine**, the aliphatic carbons are observed at 6.5 ppm (C1), 22.5 ppm (C2), 43.9 ppm (C3) and 57.7 ppm (C7). The signals at a higher field, associated with the aromatic carbons, are observed at 139.6 ppm (C4), 107.5 ppm (C5) and 153.4 ppm (C6) for **MCM-41-aminopyridine**. For **MCM-41-methylaminopyridine**, these signals are found at 155.2 ppm (C4), 108.5 ppm (C5) and 139.5 ppm (C6).[27] The MCM-41-guanidine spectrum was already assigned before.[13]

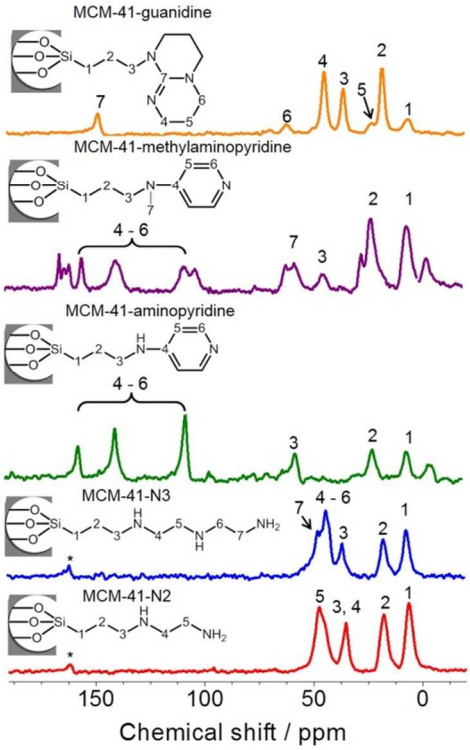

Fig. 2 ^{13}C CPMAS NMR spectra of MCM-41 and amine-functionalised samples.

N_2 sorption experiments were performed to evaluate the pore features of MCM-41 and their changes upon post-synthetic functionalisation (Fig. 3 and Fig. S1, see ESI†). Fig. 3 shows typical type IV isotherms for MCM-41, **MCM-41-N2** and **MCM-41-N3.**[28] The isotherms for **MCM-41-N2** and **MCM-41-N3** show a significant reduction of the pore volume but the same type IV feature as that of non-functionalised MCM-41, indicating that upon functionalisation the ordered structures of MCM-41 remain. In contrast, very low surface areas for **MCM-41-aminopyridine**, **MCM-41-methylaminopyridine** and **MCM-41-guanidine** (Table 1) were obtained, suggesting that the mesoporous structure of MCM-41 might be damaged or that the pores were completely blocked upon functionalisation.[29]

Pore size distributions, calculated from the adsorption branch of the N_2 isotherms at 77 K, are presented in Fig. 3 (inset). MCM-41 shows a pore size distribution approximately 2.7 nm; however, for **MCM-41-N2** the pore size distribution shifted to smaller values than that of MCM-41. For **MCM-41-N3** the pore size distribution shifted toward values smaller than 2.0 nm.

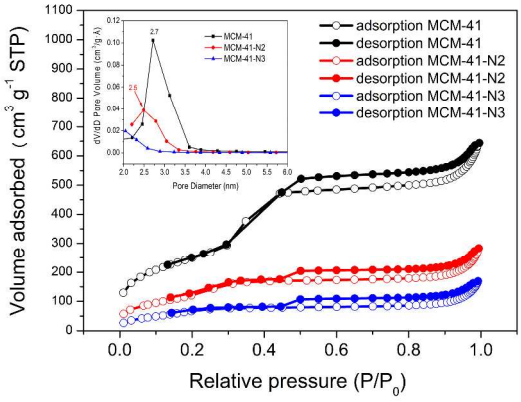

Fig. 3 N_2 Adsorption/desorption isotherms of MCM-41, **MCM-41-N2** and **MCM-41-N3** and BJH pore size distributions (inset) obtained from the adsorption branch of the isotherms.

Table 1 presents the physical properties of MCM-41 and the amine-functionalised materials. Functionalisation inside or outside the pores is expected to reduce the BET surface area, which can be confirmed by the data presented in Table 1. In addition, a reduction in pore volume (V_p) and pore diameter (D_{BJH}) is an indication that the functionalisation has, at least, partially occurred inside the pores. However, these pores were not completely blocked because the isotherms maintained the type IV features. For **MCM-41-aminopyridine**, **MCM-41-methylaminopyridine** and **MCM-41-guanidine**, the BET surface areas and pore volumes were drastically reduced (Table 1). The nitrogen and chlorine contents are summarised in Table 1.

From transmission electron microscopy (TEM) (see ESI†, Fig. S2) of MCM-41, **MCM-41-N2**, **MCM-41-N3**, **MCM-41-methylaminopyridine** and **MCM-41-guanidine**, ordered mesoporous structures of hexagonal symmetry can be observed only for **MCM-41-N2** and **MCM-41-N3**. These patterns are not observed for **MCM-41-methylaminopyridine** and **MCM-41-guanidine**, suggesting that most likely the mesoporous structure of MCM-41 was damaged, instead of pore blocking by the molecules as was noted previously.

Table 1 Physical properties of the materials

Material	S_{BET} (m^2 g^{-1})	V_p (cm^3 g^{-1})	D_{BJH} [b] (nm)	N contents (mmol g^{-1})	Amine surface density (amino group/nm^2)	CO_2 capacity (mmol g^{-1} sorbent)[c]	Amino efficiency (mol CO_2/mol N)	ΔH_{ads} [d] (kJ mol^{-1})
MCM-41	856	0.95	2.7	–	–	0.50	–	– 20
MCM-41-NH_2[a]	17	0.04	–	2.50	88.50	1.01	0.404	– 98[a]
MCM-41-N2	392	0.39	2.5	2.50	3.87	0.96	0.768[e]	– 61
MCM-41-N3	266	0.24	< 2.0	3.50	7.93	1.01	0.867[e]	– 54
MCM-41-Cl	750	0.71	2.6	0.89[f]	–	–	–	–
MCM-41-aminopyridine	3.7	0.02	N. A[g]	2.00	–	0.07	–	–
MCM-41-methylaminopyridine	8	0.04	N. A[g]	0.50	–	0.36	–	–
MCM-41-guanidine	1	0.00	N. A[g]	1.70	–	0 40	–	–

[a] Data from ref. 5. [b]Calculated from the adsorption branch using the BJH method. [c]CO_2 capacity obtained at 30 ºC and 1 bar. [d] Obtained at zero coverage. [e]The molar capacity was normalised to the number of N atoms present in each molecule. [f]Cl content (mmol g^{-1}) determined from volumetric method. [g] N. A. – not available

To confirm whether the mesoporous structure was damaged after functionalisation with 4-aminopyridine and 4-(methylamino)pyridine, as was observed for **MCM-41-guanidine**,[13] X-ray diffraction was performed (Fig. 4). The diffractograms of **MCM-41**, **MCM-41-N2** and **MCM-41-N3** were also included in Fig. 4 for comparison. The XRD patterns of MCM-41, **MCM-41-N2** and **MCM-41-N3** show three low-angle reflections typical of a hexagonal array that can be indexed as the (100), (110) and (200) Bragg peaks. Conversely, the XRD patterns of **MCM-41-aminopyridine** **MCM-41-methylaminopyridine** show no reflections. The loss of the d_{100} peak indicates that the functionalisation with 4-(methylamino)pyridine damaged the mesoporous structure of MCM-41, probably due to the higher basicity of 4-aminopyridine and 4-(methylamino)pyridine.[30] The same was observed for **MCM-41-guanidine**.[13]

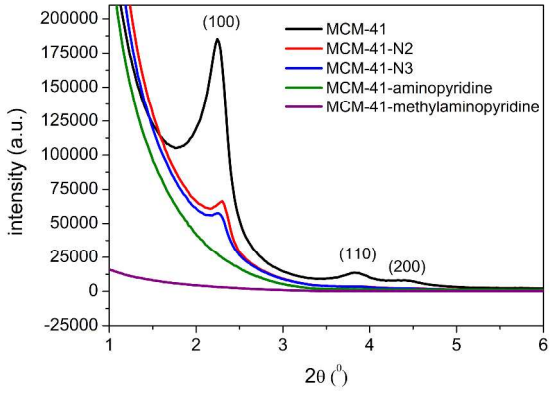

Fig. 4 X-ray diffraction patterns for MCM-41 and amine-functionalised samples.

CO_2 and CH_4 adsorption and calorimetry

It is well known that amino groups anchored onto mesoporous materials can improve CO_2 adsorption capacity due to acid–base interactions between CO_2 and the amino groups immobilised onto the external surface or within the pores of the solid material.[31] CAM-B3LYP/6-311++G(2d,2p) calculations for the same set of amines we anchored onto the MCM-41 surface showed an almost linear correlation between the CO_2 interaction energies and the amine basicities to form the zwitterion. The stronger bases showed higher interaction energies with CO_2.[20] For the same set of amines investigated in the present work, we would expect to find different behaviour among them towards CO_2 sorption.

The CO_2 and CH_4 isotherms recorded at 30 °C for MCM-41 and for the amine-functionalised materials are presented in Figs. 5 and 6. At high pressures, all amine-functionalised materials show lower CO_2 sorption capacity than that of MCM-41 (Fig. 5). This is probably due to the reduction of the pore volume of the functionalised materials which could increase the resistance to CO_2 diffusion into the pores of these materials. Therefore, in the high-pressure regime, the isotherms reflect a physical adsorption of CO_2. In contrast, at low pressures **MCM-41-N2** and **MCM-41-N3** show higher CO_2 sorption capacity than either MCM-41 or the other amine-functionalised materials. At 1.0 bar, the amount of CO_2 (n_{ads}/mmol g^{-1}) adsorbed onto **MCM-41-N2** and **MCM-41-N3** is approximately twice the amount adsorbed onto MCM-41 (Table 1). In the amino-functionalised materials, the higher CO_2 adsorption capacity is due to the reaction of this molecule with the basic amino groups anchored onto MCM-41. Thus, the isotherm profiles in this region could be due to both physisorption and chemisorption processes of CO_2. In contrast, **MCM-41-aminopyridine**, **MCM-41-methylaminopyridine** and **MCM-41-guanidine** present a smaller CO_2 adsorption capacity than MCM-41. This result may reflect the fact that the mesoporous structures of **MCM-41-aminopyridine**, **MCM-41-methylaminopyridine** and **MCM-41-guanidine** were destroyed upon functionalisation and, most importantly, after CO_2 adsorption, there would be no acidic hydrogen to be transferred to a second amine, as required by the accepted mechanism.[32] Although **MCM-41-aminopyridine** has one secondary amino group, its basicity is too low to interact with CO_2. Thus, we will focus our discussion on the CO_2 adsorption capacities of **MCM-41-N2** and **MCM-41-N3** and compare them with **MCM-41-NH_2** (aminopropyl), which was previously published.[5]

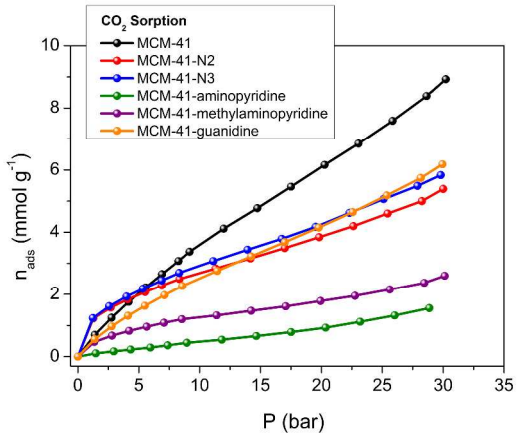

Fig. 5 CO_2 sorption for MCM-41 and the amine-functionalised samples at 30 °C.

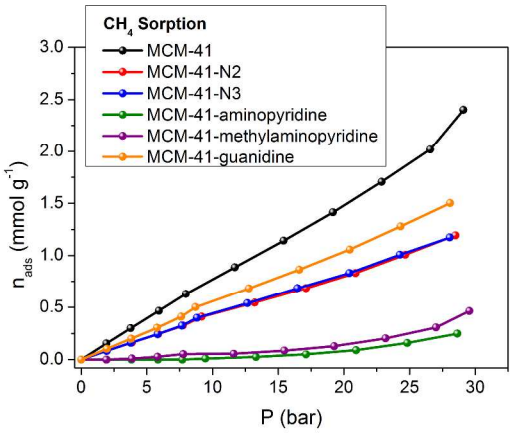

Fig. 6 CH_4 sorption for MCM-41 and the amine-functionalised samples at 30 °C.

The sorption behaviour of the amino-functionalised materials was also evaluated towards CH_4 (Fig. 6). As expected, pure MCM-41 has greater affinity for CO_2 than for CH_4 (Figs. 5 and 6). This may be attributed to either the higher quadrupole moment of CO_2[33,34] or the formation of hydrogen bonds between CO_2 and the silanol groups (Si-OH) of MCM-41.[35] The same behaviour was observed for amine-functionalised materials, but the amount of CH_4 adsorbed was less than with MCM-41. Therefore, **MCM-41-N2** and **MCM-41-N3** could be used to trap CO_2 from natural gas at low pressures.

To assess the CO_2 capture performance by the amine-functionalised materials prepared in this work, the amino efficiency was determined at 1 bar of CO_2[31], Table 1. The amino efficiency has been defined as the number of moles of CO_2 adsorbed per mole of amino groups and gives an indication of the fraction of the amino groups anchored onto MCM-41 that chemically interact with CO_2. As **MCM-41-N2** and **MCM-41-N3** have more than one amino group that could in principle contribute to the molar adsorption capacity, we normalised the amino efficiency to the number of N atoms present in each molecule as performed by Puxty *et al.*[36] For a monoamine, a maximum value of 0.5 is expected considering that two moles of amine is consumed by one mol of adsorbed CO_2.[31] In our previous work, a value of 0.404 was found for MCM-41

functionalised with an aminopropyl group.[5] The values higher than 0.5 (Table 1) found for **MCM-41-N2** and **MCM-41-N3** suggest that more than one amino group is participating in the adsorption process. The behaviour of primary *vs.* secondary amines towards CO_2 adsorption has been investigated by Sayari *et al.* who showed that secondary monoamines have weaker interactions with CO_2 than primary monoamines.[16] Additionally, Ma´mum *et al.* showed that at low CO_2 loading, primary amines react faster than secondary ones, which could be associated with a lower heat of reaction for the secondary amines.[18] However, Puxty *et al.*[36] investigated the CO_2 absorption capacity of aqueous amine solutions for 76 different amines and showed that the basic strength or pK_a of the amine will affect how far the reaction can go to products. They also concluded that weak amines will not achieve a total amino efficiency (0.5-1.0) and for polyamines, amino groups with low pK_a values will be only spectators and will not contribute to the overall absorption capacity.

Differential heats of adsorption were obtained for MCM-41, **MCM-41-N2** and **MCM-41-N3** (Fig. 7). The maximum heats of adsorption were –61.6 kJ mol^{-1} (**MCM-41-N2**), –54.6 kJ mol^{-1} (**MCM-41-N3**) and –20 kJ mol^{-1} (MCM-41). For comparison, we also included the differential heat of adsorption of **MCM-41-NH$_2$** (aminopropyl) (–98 kJ mol^{-1}) (Table 1). Differential heats of adsorption decrease as the number of secondary amino groups increases. Upon increasing CO_2 pressure, the enthalpies of adsorption of the amine-functionalised materials decrease to a value close to the one obtained for MCM-41. From these data, we can estimate the pressure where the amino groups might be saturated with CO_2, which is approximately 3 bars. Thus, at pressures higher than these values, the physisorption process might predominate over chemisorption.

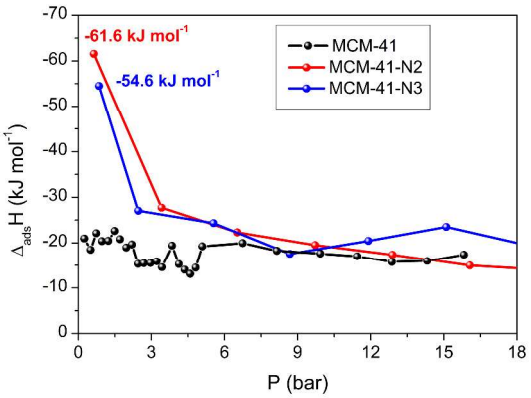

Fig. 7 Differential heats of adsorption of CO_2 for MCM-41, **MCM-41-N2** and **MCM-41-N3**.

Theoretical studies

The basicities of the primary and secondary amino groups of the molecules anchored onto MCM-41 in this work were simulated by calculations of the relative proton affinities of N^1-ethylethane-1,2-diamine ($CH_3CH_2NH(CH_2)_2NH_2$) and N^1-(2-aminoethyl)-N^2-ethylethane-1,2-diamine ($CH_3CH_2NH(CH_2)_2NH(CH_2)_2NH_2$), using the wB97x-D/6-311++G(d,p) method (see ESI†, Table S1).

The relative proton affinities of the secondary amino groups are much higher than those of the primary amino groups, indicating that the secondary amino groups would be more effective in the interactions with CO_2 molecules. To confirm this hypothesis, we also calculated the relative stabilities of the carbamates resulting from the interaction of CO_2 with both the primary and secondary amino groups of the same amines (see ESI†, Table S2). The relative stabilities of the primary and the secondary carbamates are indeed very similar. For N^1-ethylethane-1,2-diamine, the secondary carbamate is 1.8 kJ mol^{-1} more stable than the primary one. For N^1-(2-aminoethyl)-N^2-ethylethane-1,2-diamine, the primary carbamate are more stable than the secondary ones (from the two possible secondary carbamates) by 3.8 kJ mol^{-1} on average (on a ΔG basis at 298K). With such small energy differences between the primary and secondary carbamates, we expect that both could be found in the present systems. The lower energy difference for the carbamates compared to the proton affinity of the secondary amines is probably due to the formation of stabilizing intramolecular hydrogen bonds between the carbamate group and the hydrogen donor amino groups (see see ESI†, Table S1 and S2). Thus, the strong intramolecular hydrogen bonds found in both primary and secondary carbamates cause a levelling effect in the relative energy. Therefore, based on the relative energies of the carbamates, the formation of either primary or secondary carbamates in these systems cannot be excluded despite the difference in the basicity of the primary and secondary amino groups.

The reduction of the differential heats of adsorption as the number of amino group increases (Fig. 7) cannot be attributed to different behaviours between the primary and secondary amino groups towards CO_2 adsorption because the relative energies of the primary and secondary carbamates are close. Most likely, this reduction might be associated with a simultaneous CO_2 adsorption on both amino groups. It is reasonable to assume that the simultaneous CO_2 adsorption on both primary and secondary amino groups will release a smaller heat of adsorption than that released for the adsorption on either the primary or secondary amino groups.

Conclusions

CO_2 and CH_4 adsorption studies were conducted using commercially available MCM-41 functionalised with [3-(2 aminoethylamino)propyl] trimethoxysilano, N^1-(3-trimethoxysilylpropyl)diethylenetriamine, 4-aminopyridine, 4-(methylamino)pyridine, 1,5,7-triazabicyclo[4.4.0]dec-5-ene (guanidine). ^{29}Si and ^{13}C solid state nuclear magnetic resonances showed that all molecules were covalently bounded onto MCM-41. However, X-ray diffraction and transmission electron microscopy revealed that upon functionalisation the mesoporous structure of MCM-41 was destroyed in **MCM-41-aminopyridine**, **MCM-41-methylaminopyridine** and **MCM-41-guanidine**. Negligible amounts of CH_4 were adsorbed on the amine-functionalised materials. In contrast, CO_2 adsorption measurements at 1.0 bar and 30 ^{o}C showed that the amount of CO_2 (n_{ads}/mmol g^{-1}) adsorbed on **MCM-41-N2** and **MCM-41-N3** is *approximately* twice the amount adsorbed on MCM-41. For **MCM-41-aminopyridine**, **MCM-41-methylaminopyridine**, **MCM-41-guanidine,** the CO_2 adsorption capacities were smaller than for adsorption on MCM-41 at the same conditions. This result could be related to structural damage of MCM-41 upon

functionalisation and, most importantly, to the absence of an acidic hydrogen atom in these amines necessary to be transferred to a second amine. The amino efficiency of **MCM-41-N2** and **MCM-41-N3**, normalised by the number of N atoms present in each molecule, showed that both primary and secondary amino groups contribute to the CO_2 adsorption on the materials. The proton affinity, calculated using the wB97x-D/6-311++G(d,p) method, is higher for the secondary amino groups than for the primary ones; however, the stabilities of the primary and secondary carbamates on a ΔG basis are similar, showing that both groups can interact with CO_2. Differential heats of adsorption are –61.6 kJ mol^{-1} (**MCM-41-N2**), –54.6 kJ mol^{-1} (**MCM-41-N3**) and –20 kJ mol^{-1} (MCM-41) indicating a chemical interaction between CO_2 and the amine-functionalised materials at low pressures. The differential heat of adsorption decreases as the number of secondary amino groups increases (e.g., for MCM-41 functionalised with aminopropyl group it is –98 kJ mol^{-1}, ref. 5), probably due to simultaneous CO_2 adsorption on secondary and primary amino groups.

Acknowledgements

The authors gratefully acknowledge FAPERJ (JCNE, CNE and Pensa Rio grants), CNPq (Jovens Pesquisadores em Nanotecnologia grant number 550572/2012-0 and Universal grant number 478302/2012-6) and CAPES (T.C.S. fellowship) for financial support. C.M.R. and J.W.M.C. are recipients of CNPq research fellowships. We thank Prof. Victor Marcos Rumjanek (IQ-UFRRJ, Brazil) for the Solid State NMR spectra and the Multiuser Materials Characterisation Laboratory (http://www.uff.br/lamate/).

Notes and references

[a] *Instituto de Química, Universidade Federal Fluminense, Campus do Valonguinho, CEP 24020-141, Niterói, Rio de Janeiro, Brazil. E-mail: cmronconi@id.uff.br*

[b] *Laboratoire Chimie Provence, Universités d'Aix-Marseille I, II & III - CNRS, UMR 6264, Centre de Saint Jérôme, 13397 Marseille cedex 20, France.*

Electronic Supplementary Information (ESI) available. See DOI: 10.1039/b000000x/

1 IPCC, 2014: Summary for Policymakers, in Climate Change 2014, Mitigation of Climate Change. Contribution of Working Group III to the Fifth Assessment Report of the Intergovernmental Panel on Climate Change [O. Edenhofer, R. Pichs-Madruga, Y. Sokona, E. Farahani, S. Kadner, K. Seyboth, A. Adler, I. Baum, S. Brunner, P. Eickemeier, B. Kriemann, J. Savolainen, S. Schlömer, C. von Stechow, T. Zwickel and J. C. Minx (eds.)]. Cambridge University Press, Cambridge, United Kingdom and New York, NY, USA.

2 T. C. Santos and C. M. Ronconi, *Rev. Virtual Quim.*, 2014, **6**, 112.

3 R. R. Bottoms (Girdler Corp.), "Separating acid gases," U.S. Patent 1783901, 1930.

4 G. T. Rochelle, *Science*, 2009, **325**, 1652.

5 M. R. Mello, D. Phanon, G. Q. Silveira, P. L. Llewellyn and C. M. Ronconi, *Micropor. Mesopor. Mater.*, 2011, **143**, 174.

6 A. Heydari-Gorji, Y. Yang and A. Sayari, *Energ. Fuels*, 2011, **25**, 4206.

7 L. Zhou, J. Fan, G. Cui, X. Shang, Q. Tang, J. Wang and M. Fan, *Green Chem.*, 2014, **16**, 4009.

8 F. Su, C. Lu, S.-C. Kuo and W. Zeng, *Energ. Fuels*, 2010, **24**, 1441.

9 Y. Hu, W. M. Verdegaal, S.-H. Yu and H.-L. Jiang, *ChemSusChem*, 2014, **7**, 734.

10 X. Zhao, X. Hu, R. Bai, M. Fan and M. Luo, *J. Mater. Chem. A*, 2013, **1**, 6208.

11 L. Stevens, K. Williams, W. Y. Han, T. Drage, C. Snape, J. Wood and J. Wang, *Chem. Eng. J.*, 2013, **215**, 699.

12 A. Sayari, A. Heydari-Gorji and Y. Yang, *J. Am. Chem. Soc.*, 2012, **134**, 13834.

13 A. L. de Lima, A. Mbengue, R. A. S. San Gil, C. M. Ronconi and C. J. A. Mota, *Catal. Today*, 2014, **226**, 210.

14 G. Q. Silveira, M. D. Vargas and C. M. Ronconi, *J. Mater. Chem.*, 2011, **21**, 6034.

15 G. Q. Silveira, R. S. da Silva, L. P. Franco, M. D. Vargas and C. M. Ronconi, *Micropor. Mesopor. Mater.*, 2015, **206**, 226.

16 A. Sayari, Y. Belmabkhout and E. Da'na, *Langmuir*, 2012, **28**, 4241.

17 S. Ma'mun, J. P. Jakobsen and H. F. Svendsen, *Ind. Eng. Chem. Res.*, 2006, **45**, 2505.

18 S. Ma'mun, V. Y. Dindore and H. F. Svendsen, *Ind. Eng. Chem. Res.*, 2007, **46**, 385.

19 S. Builes and L. F. Vega, *J. Phys. Chem. C*, 2012, **116**, 3017.

20 E. Orestes, C. M. Ronconi and J. W. de M. Carneiro, *J. Phys. Chem. Chem. Phys.*, 2014, **16**, 17213.

21 A. D. Wiersum, C. Giovannangeli, D. Vincent, E. Bloch, H. Reinsch, N. Stock, J. S. Lee, J.-S. Chang and P. L. Llewellyn, *ASC Combin. Sci.,* 2013, **15**, 111.

22 E. W. Lemmon, H. M. McLinden, Reference Fluid Thermodynamic and Transport Properties, REFPROP 8.0, National Institute of Standards and Technology: Gaithersburg, MD, 2007.

23 J.-D. Chai and M. Head-Gordon, *Phys. Chem. Chem Phys.*, 2008, **10**, 6615.

24 Gaussian 09, Revision A.01, M. J. Frisch, G. W. Trucks, H. B. Schlegel, G. E. Scuseria, M. A. Robb, J. R. Cheeseman, G. Scalmani, V. Barone, B. Mennucci, G. A. Petersson, H. Nakatsuji, M. Caricato, X. Li, H. P. Hratchian, A. F. Izmaylov, J. Bloino, G. Zheng, J. L. Sonnenberg, M. Hada, M. Ehara, K. Toyota, R. Fukuda, J. Hasegawa, M. Ishida, T. Nakajima, Y. Honda, O. Kitao, H. Nakai, T. Vreven, J. A. Jr. Montgomery, J. E. Peralta, F. Ogliaro, M. Bearpark, J. J. Heyd, E. Brothers, K. N. Kudin, V. N. Staroverov, R. Kobayashi, J. Normand, K. Raghavachari, A. Rendell, J. C. Burant, S. S. Iyengar, J. Tomasi, M. Cossi, N. Rega, N. J. Millam, M. Klene, J. E. Knox, J. B. Cross, V. Bakken, C. Adamo, J. Jaramillo, R. Gomperts, R. E. Stratmann, O. Yazyev, A. J. Austin, R. Cammi, C. Pomelli, J. W. Ochterski, R. L. Martin, K. Morokuma, V. G. Zakrzewski, G. A. Voth, P. Salvador, J. J. Dannenberg, S. Dapprich, A. D. Daniels, Ö. Farkas, J. B. Foresman, J. V. Ortiz, J. Cioslowski, D. J. Fox, Gaussian, Inc., Wallingford CT, 2009.

25 ***Spartan'10***, Wavefunction, Inc., Irvine, CA.

26 S. Huh, J. W. Wiench, J.-C. Yoo, M. Pruski and V. S.-Y. Lin, *Chem. Mater.,* 2003, **15**, 4247.

27 H.-T. Chen, S. Huh, J. W. Wiench, M. Pruski and V. S.-Y. Lin, *J. Am. Chem. Soc*., 2005, **127**, 13305.

28 K. Sing, D. Everett, R. Haul, L. Moscou, R. Pierotti, J. Rouquerol and T. Siemieniewska, *Pure Appl. Chem.*, 1985, **57**, 603.

29 X. Xiaochun, S. Chunshan, M. A. John, G. M. Bruce and W. S. Alan, *Energ. Fuel.,* 2002, **16**, 1463.

30 L. B. Sun, J. Yang, J. H. Kou, F. N. Gu, Y. Chun, Y. Wang, J. H. Zhu and Z. G. Zou, *Angew. Chem. Int. Ed.*, 2008, **47**, 3418.

31 P. Bolline, S. A. Didas and C. W. Jones, *J. Mater. Chem.*, 2011, **21**, 15100.

32 M. Caplow, *J. Am. Chem. Soc.,* 1968, **24**, 6795.

33 J. Kim, A. Maiti, L.-C. Lin, J. K. Stolaroff, B. Smit and R. D. Aines, *Nat. Commun.*, 2013, **4**, 1.

34 P. Chowdhury, C. Bikkina and S. Gumma, *J. Phys. Chem. C,* 2009, **113**, 6616.

35 C. S. Srikanth and S. S. C. *Chuang, J. Phys. Chem. C,* 2013, **117**, 9196.

36 G. Puxty, R. Rowland, A. Allport, Q. Yang, M. Bown, R. Burns, M. Maeder and M. Attalla, *Environ. Sci. Technol.,* 2009, **43**, 6427.